

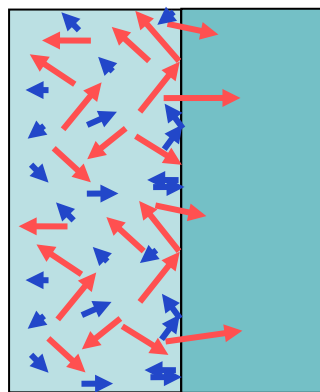
Thermoelectricity: From Atoms to Systems

Week 5: Recent Advances in Thermoelectric Materials and Physics
Lecture 5.6: Overview of Week 5, Recent reviews

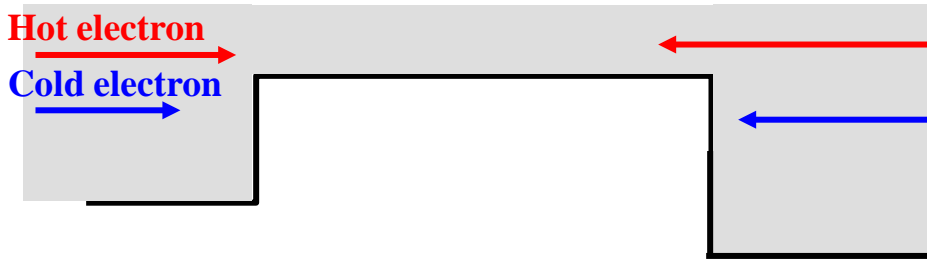
By Ali Shakouri
Professor of Electrical and Computer Engineering
Birck Nanotechnology Center
Purdue University

Thermionic (TI) vs. Thermoelectric (TE)

Lateral momentum
conservation



Energy



Cathode

Material 1

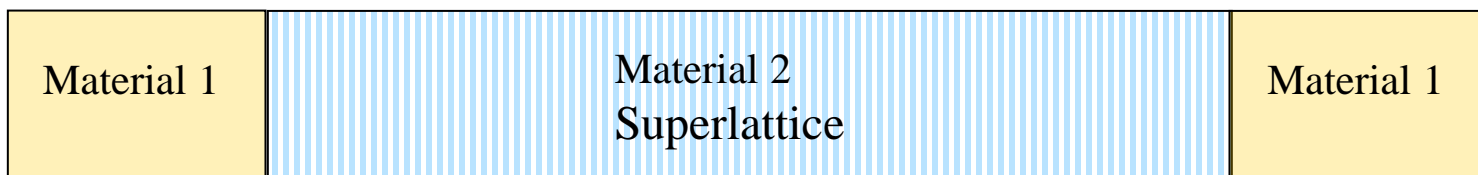
Barrier

Material 2
Single Barrier

Anode

Material 1

Thermionic: ballistic, non-linear transport

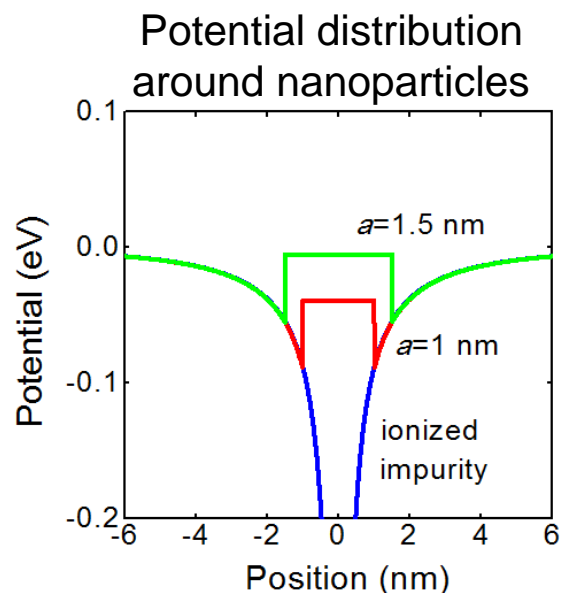
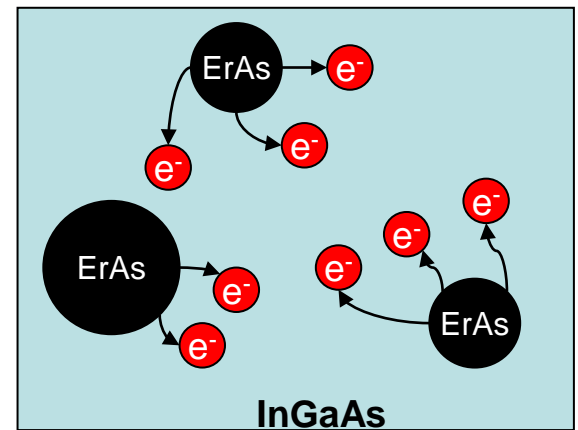
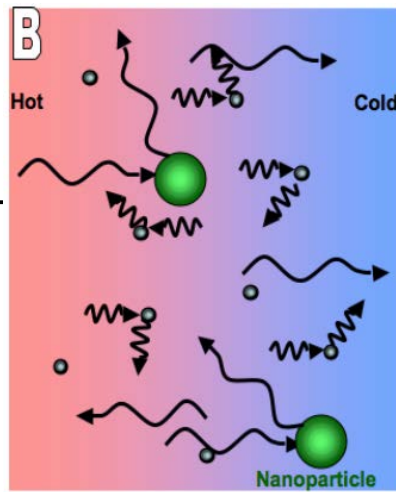
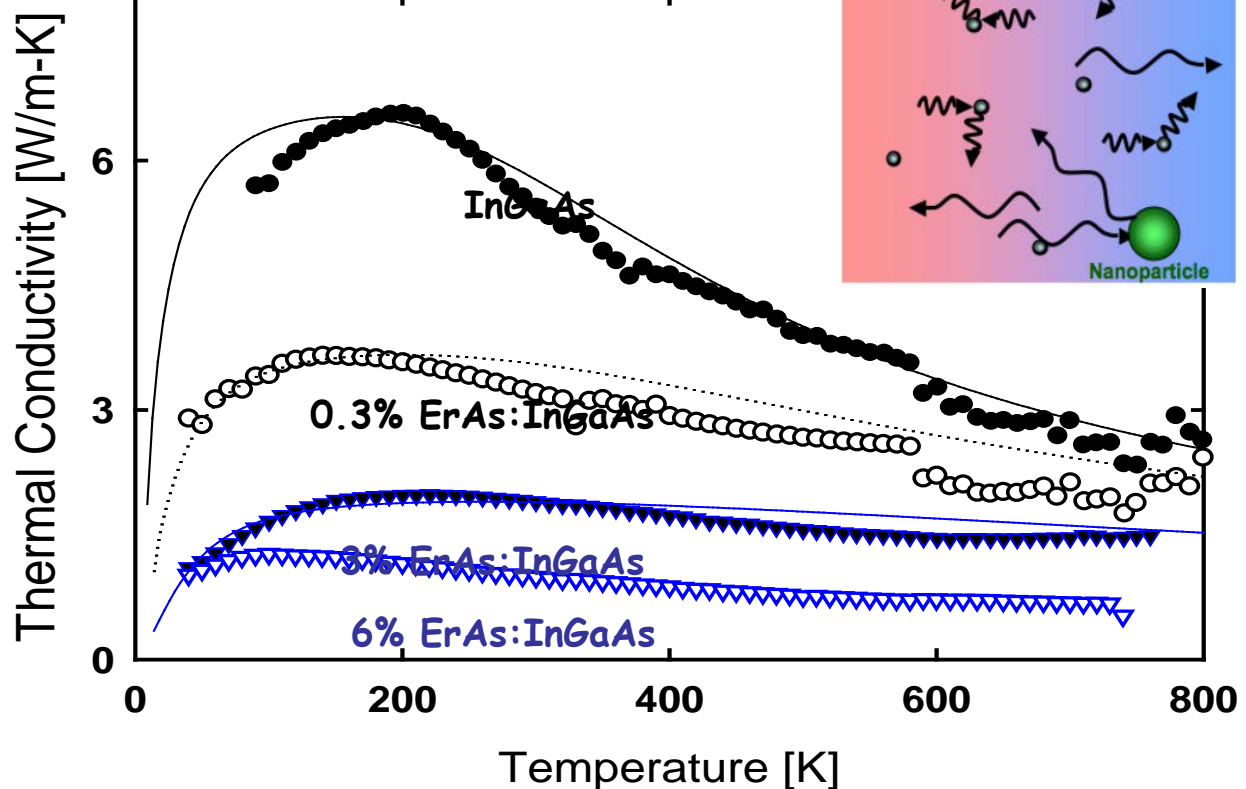


Superlattice: Linear transport: “**effective**” Seebeck coefficient

D. Vashaee, A. Shakouri, Phys. Rev. Lett., 2004

Embedded ErAs nanoparticles in InGaAs matrix

ZT~1.3-1.5 @800K



W. Kim, J. Zide et al. Physical Review Letters 2006
J-H. Bahk, et al., Applied Physics Letters 99, 072118, 2011

Material Figure-of-Merit for Thermoelectrics

$$Z = \frac{S^2 \sigma}{k}$$

$$Z = \frac{(Seebeck)^2 (\text{electrical conductivity})}{(\text{thermal conductivity})}$$

Material Figure-of-Merit $\left(\frac{\mu \cdot m^*^{1.5}}{k} \cdot T_c^{2.5} \right)$

Mobility $\mu = \left(\frac{e \tau}{m^*} \right)$

τ : scattering time

m^* : effective mass

Keyes' Relation (phonon-phonon scattering dominates k_{lattice} at high T)

$$k_{\text{latt}} T = \left(\frac{R^{3/2}}{3\gamma^2 \varepsilon^3 N_0^{1/3}} \frac{T_m^{3/2} \rho^{2/3}}{A^{7/6}} \right)$$

T_m : melting temperature, A : mean atomic weight,
 γ : Gruneisen constant, ε : fractional amplitude of interatomic thermal vibration, R : ideal gas constant, N_0 : Avogadro's number, ρ : density

Boltzmann Transport /nanoHUB simulation

1 Band Structure → 2 Scattering Properties → 3 Simulation Parameters → 4 Simulate

Material: PbTe - Lead Telluride
 Bands: 3. Single Conduction Band - Double Valence Bands

PbTe has primary conduction and valence bands at the L valley in the Brillouin zone. There is a secondary valence band at the Sigma valley, of which the band edge is about 40 meV down below the first valence band edge at 300 K. The secondary conduction band is ignored. The band gap, the band offset between the two valence bands and their effective masses are all functions of temperature (T).

Change values...

- Electron effective mass of 1st conduction band: $0.04166 + 1.237e-4 T$
- Nonparabolicity for 1st conduction band (1/eV): $1/(2.345 + 6.813e-4 T)$
- Band degeneracy of 1st conduction band: 4

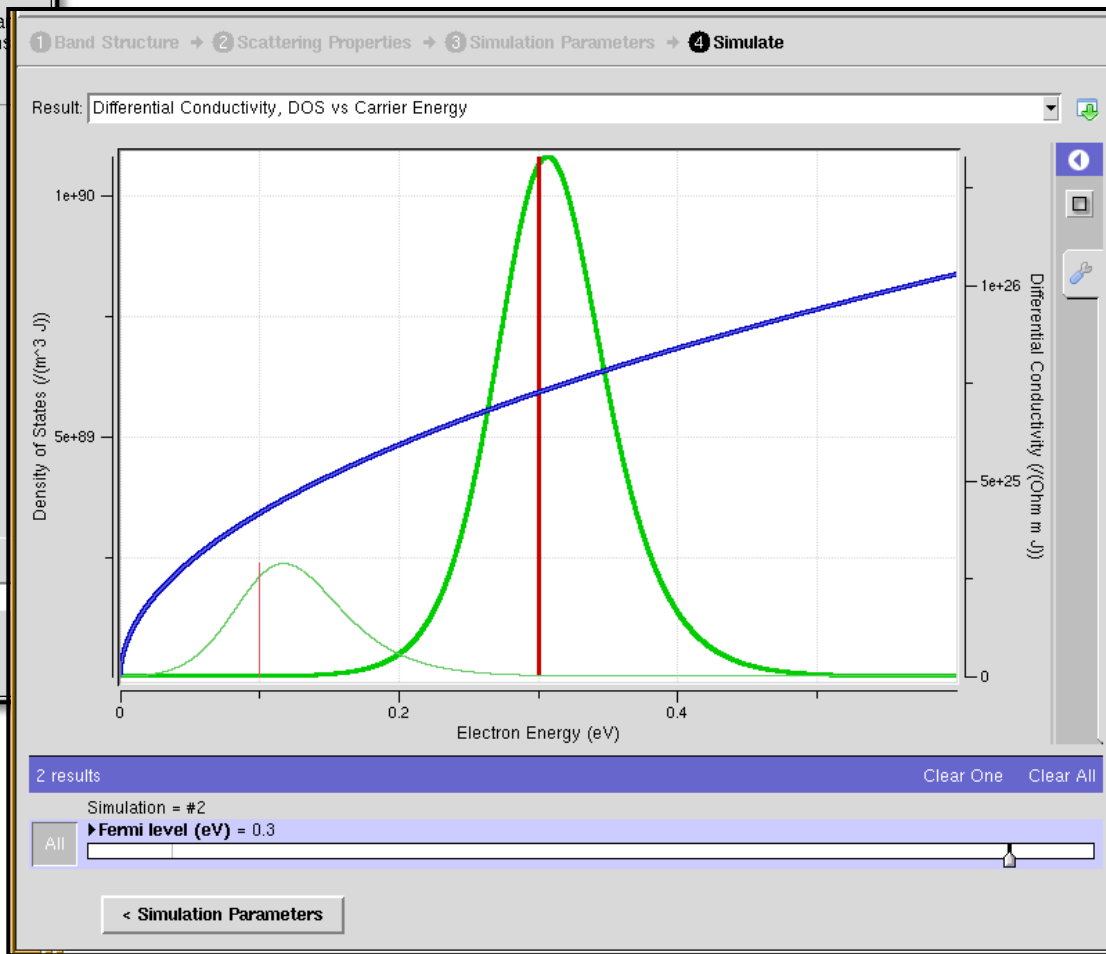
Fractional composition?: no
 x (fraction of composition) 0.5

Scattering Properties >

$S = -95 \mu\text{V/K}$
 $\sigma = 2.2e4 / \Omega\text{cm}$
 for $E_F = 0.3 \text{ eV}$

$S = -37 \mu\text{V/K}$
 $\sigma = 4.6e3 / \Omega\text{cm}$
 for $E_F = 0.1 \text{ eV}$

n-PbTe, 300 K
 Input e.g. $\tau = 0.1 \text{ ps (const.)}$



Optimum band structure for thermoelectrics

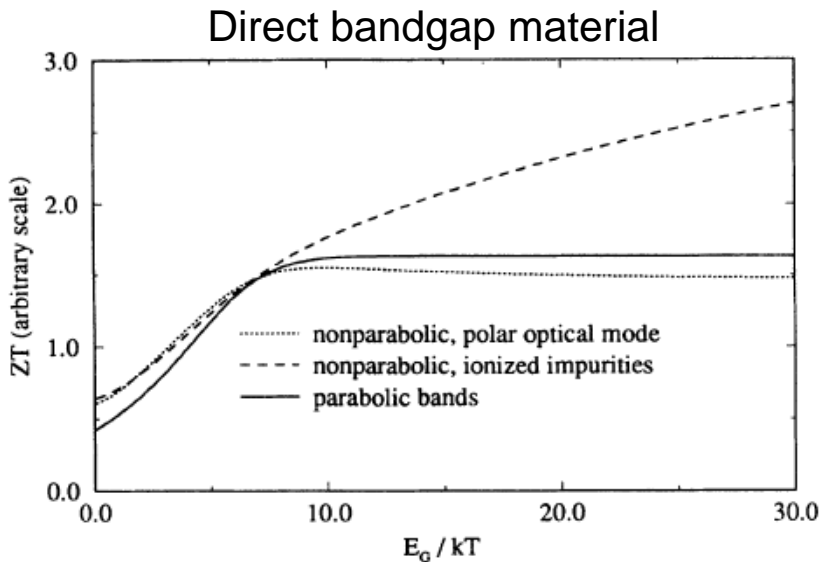
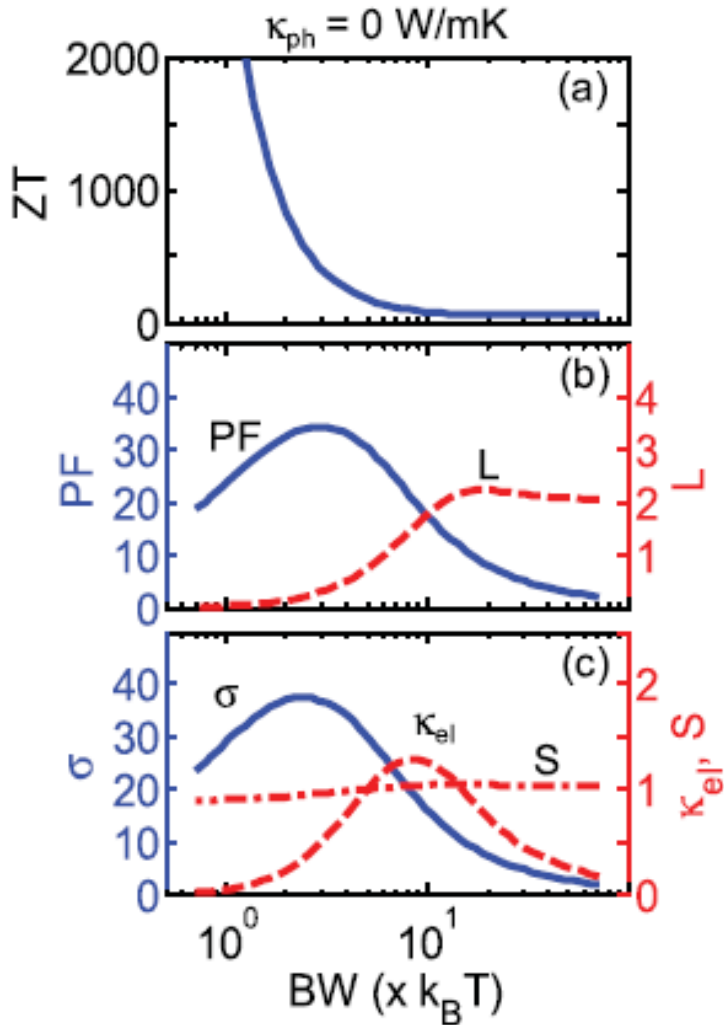


FIG. 1. Maximum value of ZT as a function of the energy band gap E_g in units of thermal energy $k_B T$, for parabolic bands and for nonparabolic bands with two different scattering mechanisms.

$$m^* = \frac{3\hbar^2}{4P^2} E_G$$

P= Kane matrix element describing direct gap material

Changwook Jeong, Raseong Kim, and Mark S. Lundstrom. J. Appl. Phys., Vol. 111, 113707, 2012.

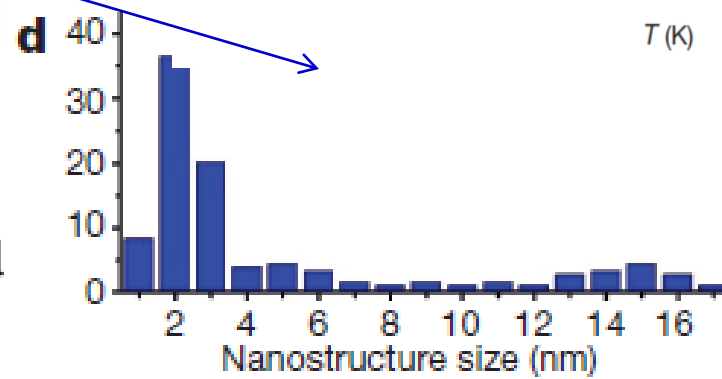
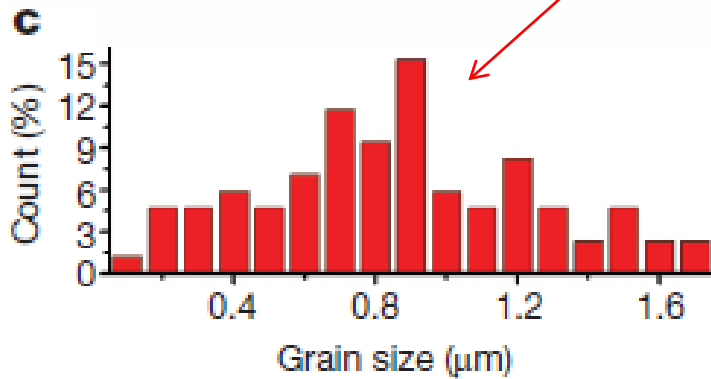
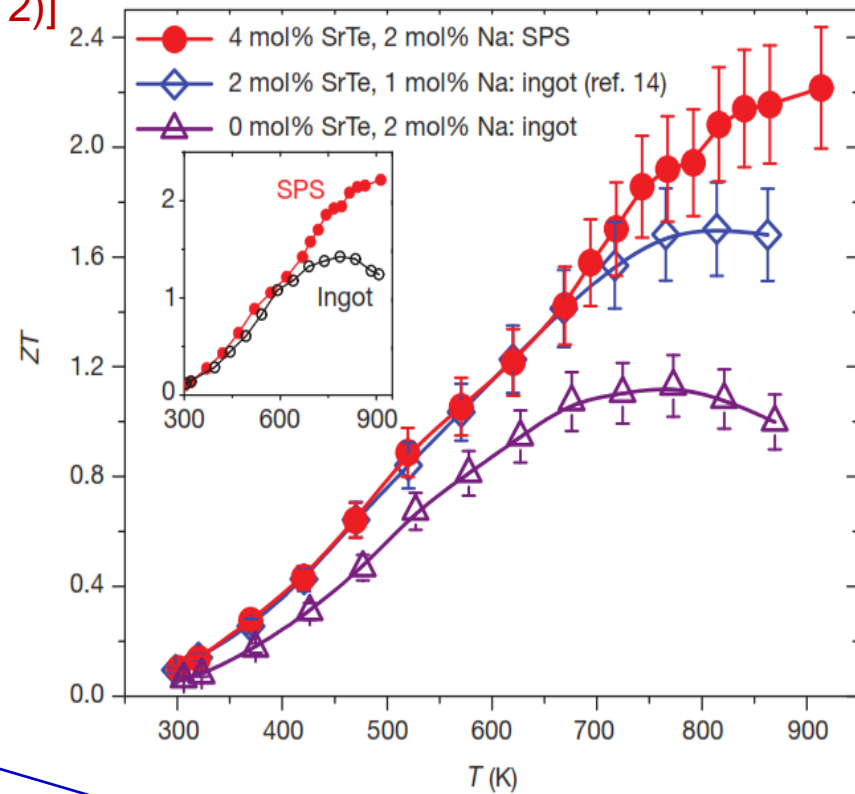
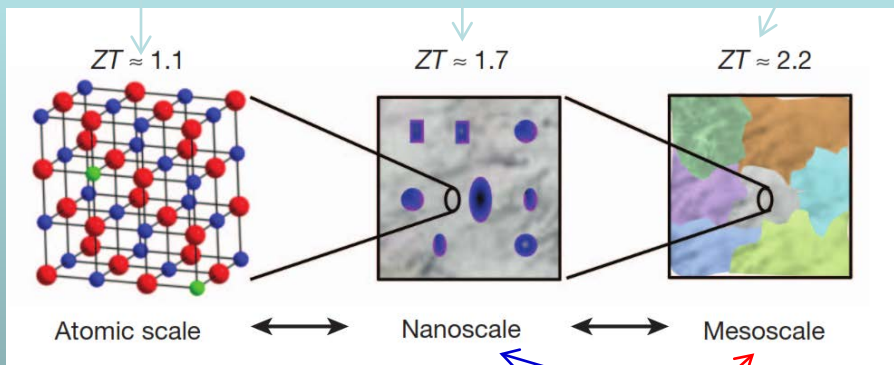
Sofo and Mahan, Phys. Rev. B 49, 4565–4570 (1994)

Record ZT~2.2 (Sept. 2012)

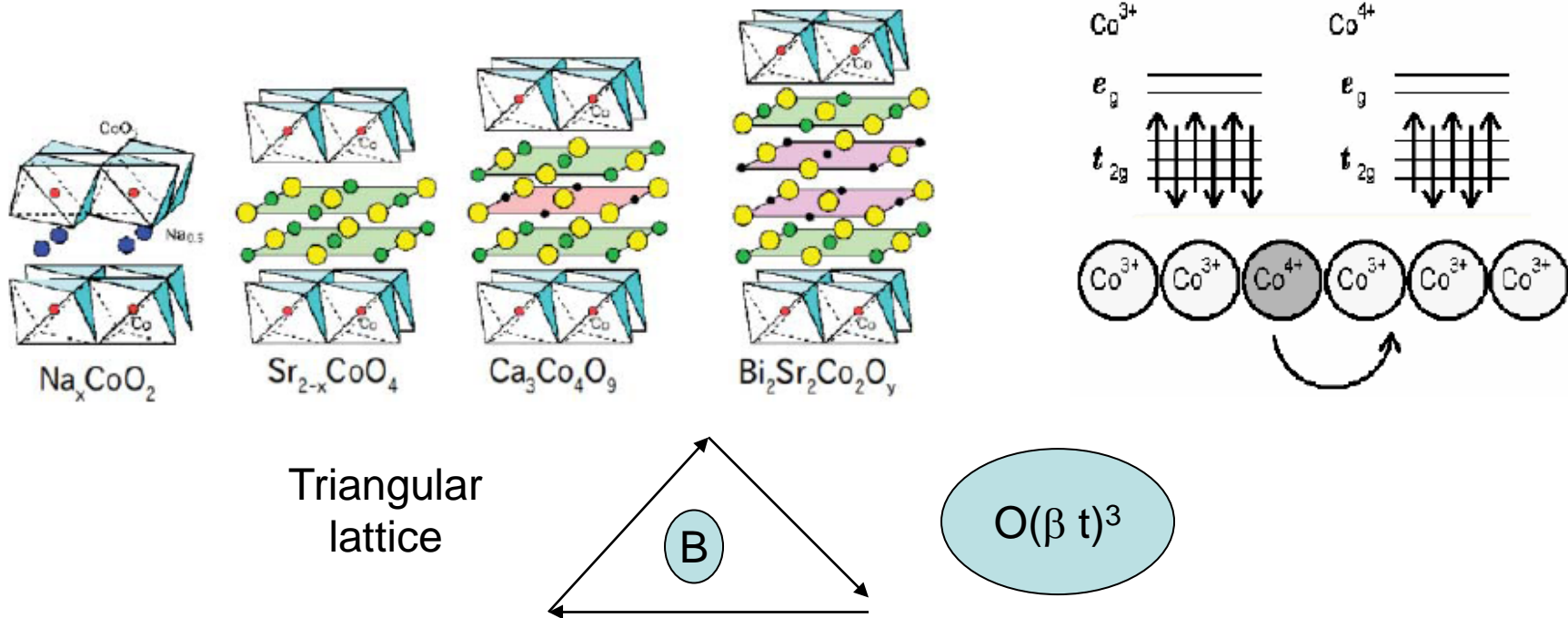
[Biswas et al.(Kanatzidis group), *Nature* 489, 414 (2012)]

Spark-plasma-sintered
Na(2%)-doped PbTe:SrTe(4%)

Na-doped PbTe Na-doped SrTe:PbTe SPS



Oxide Thermoelectrics



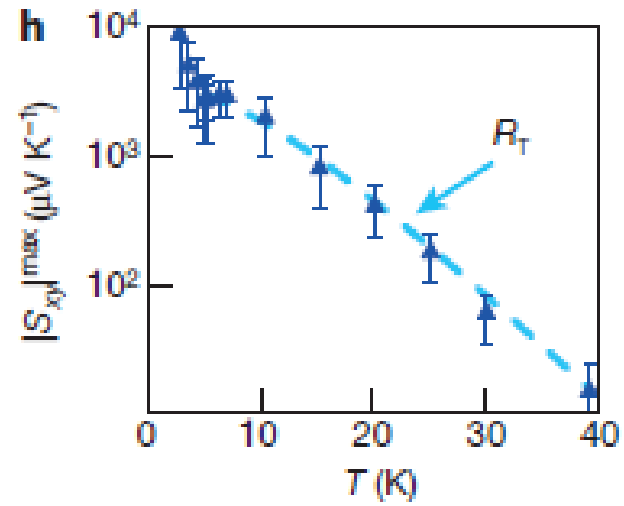
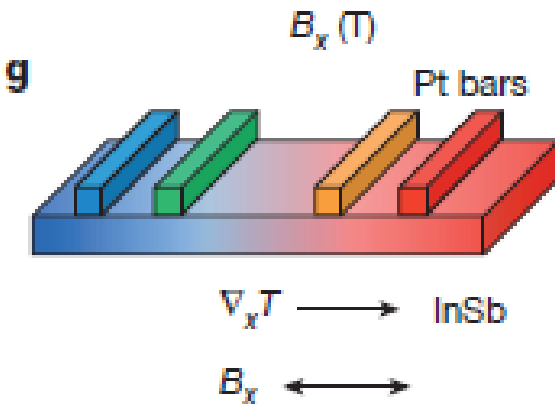
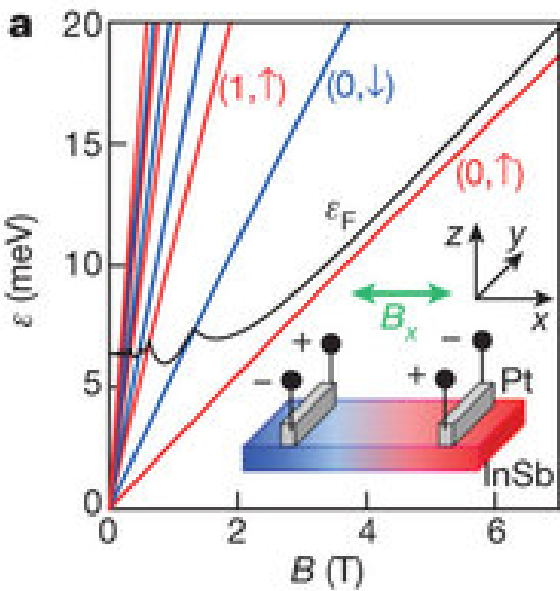
Potential cause of high power factor:

- Large **entropy of mixed $\text{Co}^{3+}/\text{Co}^{4+}$ state with low spin** (Koshibae et al.)
- There are correlation effects, geometric frustration (B.S. Shastry)
- Potential explanation of high Seebeck using standard band theory (D. Singh)

Difficult to control Na content (evaporates at high T) and decomposition at 1100 K.

K. Koumoto, Y. Wang, et al.; Annual Rev. Mat. Res., VOL 40 Pages: 363-394 2010

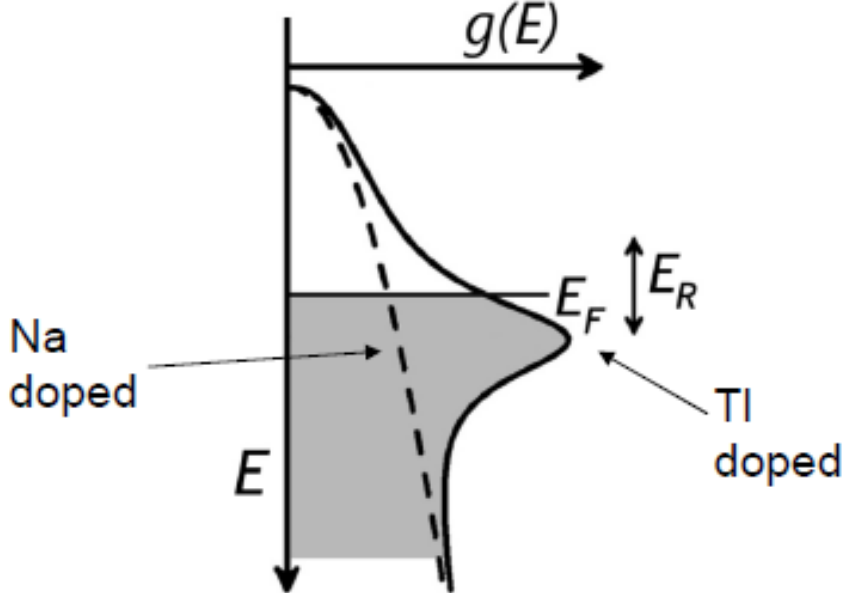
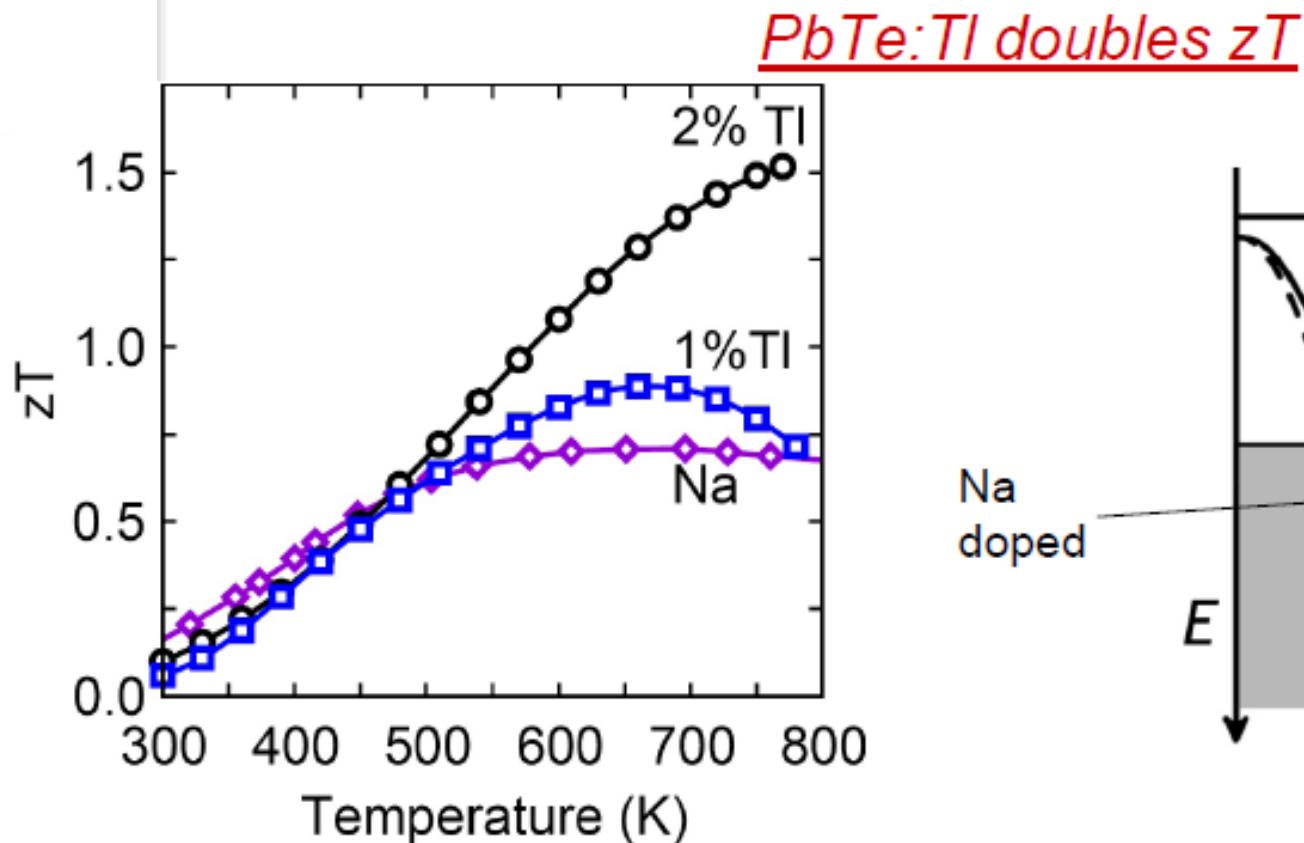
Giant Spin Seebeck



Maximum Spin Seebeck at 2.7T of the cold Pt bar.

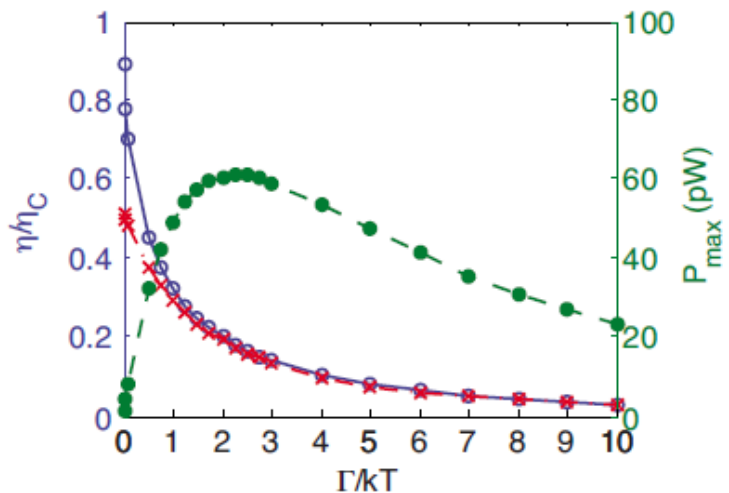
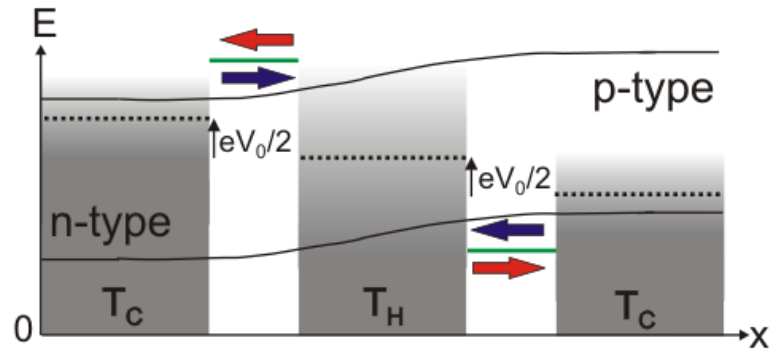
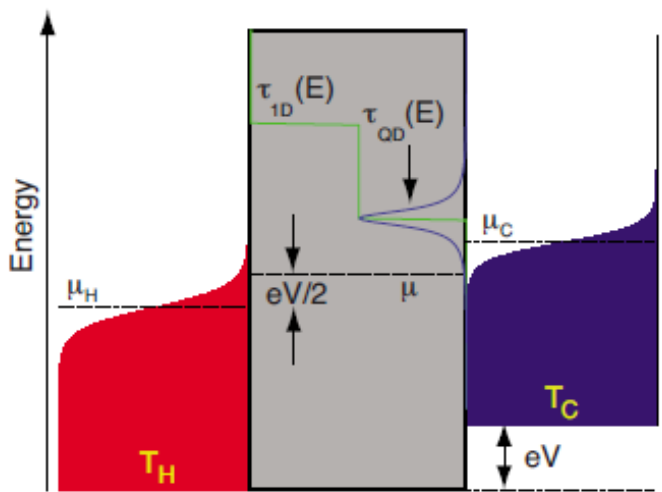
Jaworski, Heremans, et al., Giant spin Seebeck effect in a non-magnetic material. Nature (2012) 487, 7406, p. 210

Resonant State Thermoelectrics



Heremans et al. Science 321, 554, 2008

Single Level Thermoelectrics



T. E. Humphrey and H. Linke, *Phys. Rev. Lett.* **94**, 096601 (2005)

Nakpathomkun et al., *Phys. Rev. B* **82**, 235428, 2010

Phase transition; Coupling between charge and energy transports

$$\xi = \frac{Z^* T}{1 + Z^* T}$$

• ξ coupling factor between charge and energy density

• Z^* high frequency limit of figure of merit

• *B. S. Shastry,*
Rep, Prog, Phys 72,
016501, (2009)

• *Y. Ezzahri et al.*
Phys. Rev. B, 79,
184303, (2009)

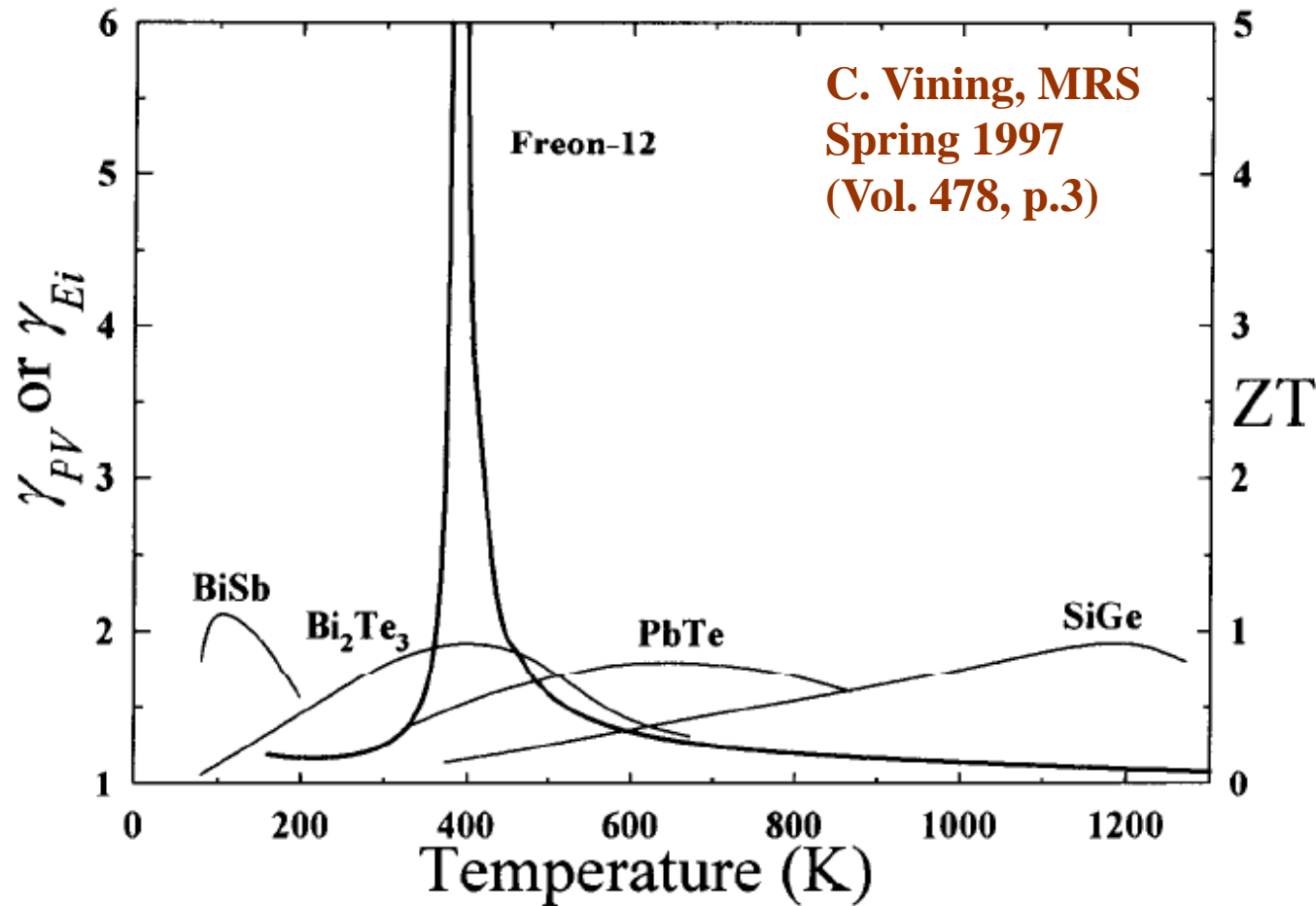
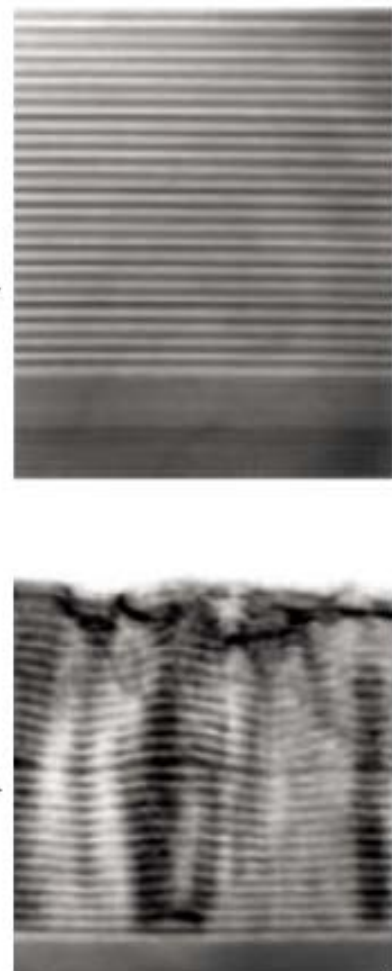
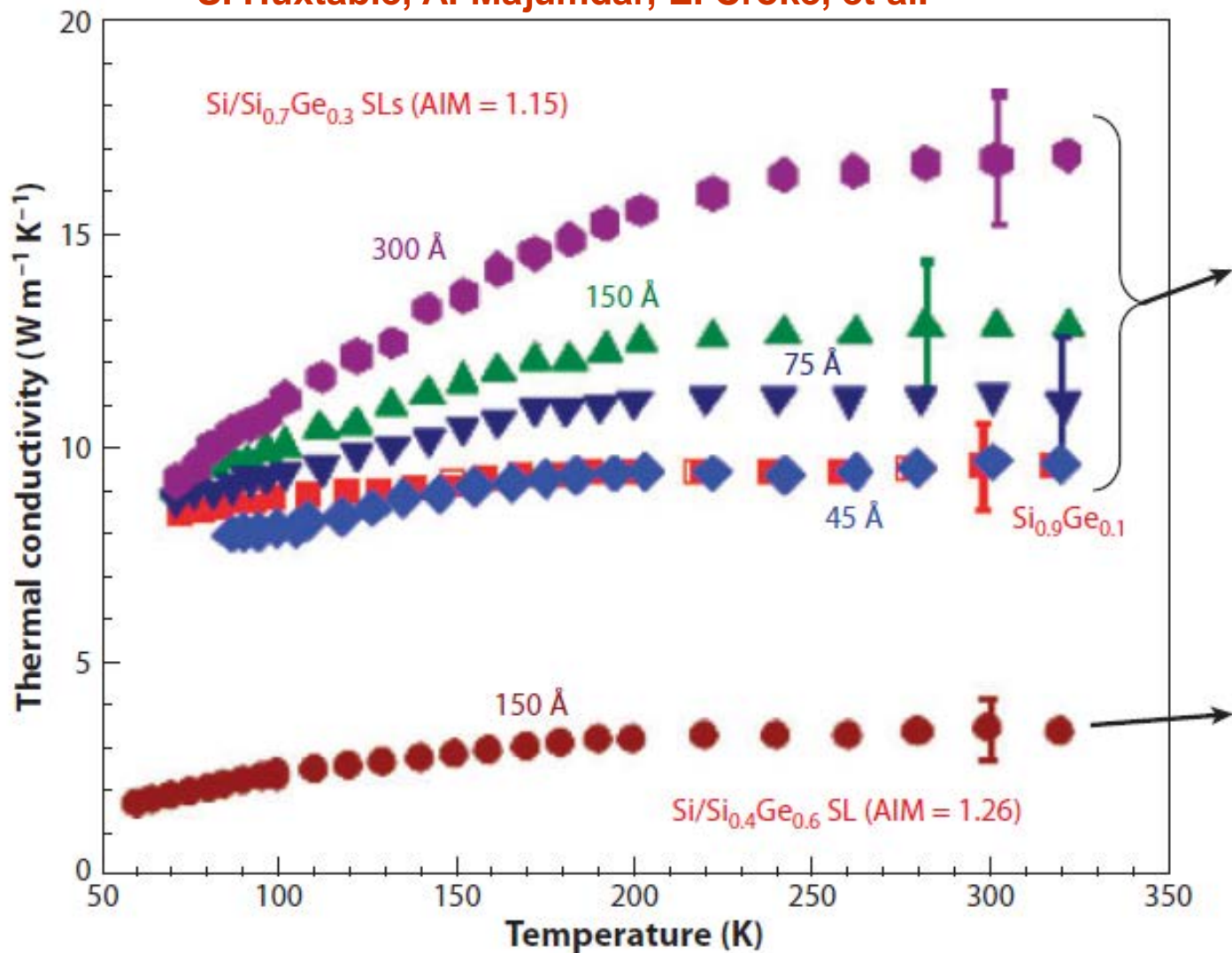


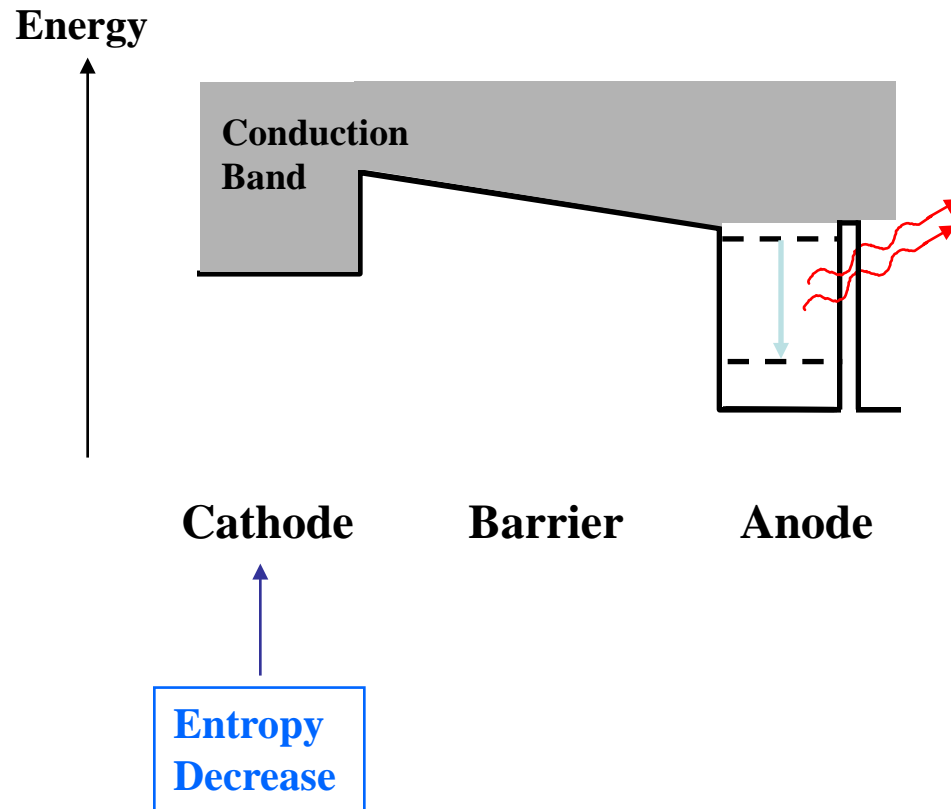
Fig. 4: Specific heat ratios, γ_{PV} for a PV system (Freon 12) and thermal conductivity ratios, $\gamma_{Ei} - 1 + ZT$, for selected n-type semiconductor alloys as a function of temperature.

SiGe/Si superlattice thermal conductivity

S. Huxtable, A. Majumdar, E. Croke, et al.



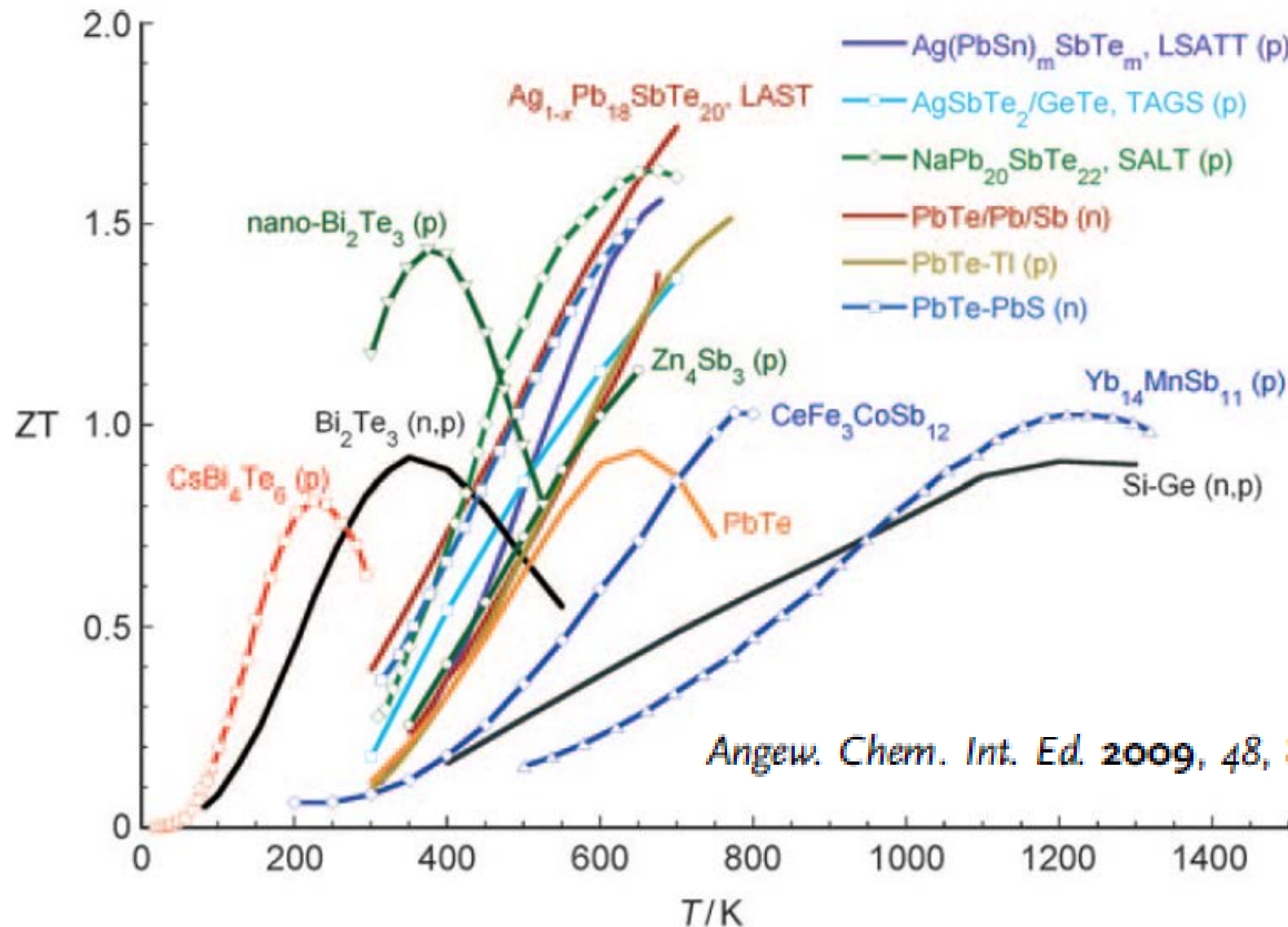
A. Shakouri, *Annual Review of Materials Research*, July 2011



Ali Shakouri and John E. Bowers, “*Heterostructure integrated thermionic refrigeration*”,
International Conference on Thermoelectrics, Dresden, Germany, August 1997

New and Old Concepts in Thermoelectric Materials

Joseph R. Sootsman, Duck Young Chung, and Mercouri G. Kanatzidis*



Angew. Chem. Int. Ed. 2009, 48, 8616–8639

The Zintl Phase $\text{Yb}_{14}\text{MnSb}_{11}$

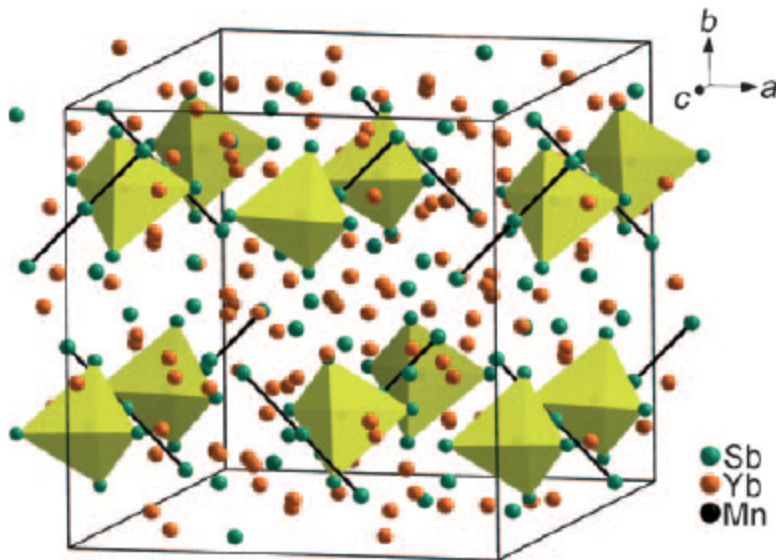


Figure 10. The cubic crystal structure of $\text{Yb}_{14}\text{MnSb}_{11}$ consists of one $[\text{MnSb}_4]^{9-}$ tetrahedral unit (yellow), one $[\text{Sb}_3]^{7-}$ ion (centers linked by black lines), four Sb^{3-} ions situated between the $[\text{MnSb}_4]^{9-}$ and $[\text{Sb}_3]^{7-}$ units, and 14 Yb^{2+} ions per formula.

Hot-pressed pellets showed electrical Conductivity of $185 \text{ } \Omega\text{cm}$ and Seebeck coefficient of $180 \mu\text{V/K}$ at 1200 K. The low thermal conductivity 0.7–0.9 W/mK in temperatures between 200–1275 K gives rise to the remarkable ZT of ~1.0 at 1200 K.

The low thermal conductivity is primarily attributed to the large lattice constant, the structural complexity, and to the ionic character bonding in the lattice.

It is possible that $\text{Yb}_{14}\text{MnSb}_{11}$ and its alloys may replace p-type Si-Ge alloys in future space missions.

S. R. Brown, S. M. Kauzlarich, F. Gascoin, G. J. Snyder, Chem. Mater. 2006, 18, 1873.

Sootsman et al., Angew. Chem. Int. Ed. 2009, 48, 8616 – 8639

Nano-enhanced (e.g. using Spark Plasma Sintering to create nanoparticle composites)

B. Poudel, Z. Ren, G. Chen, M. Dresselhaus et al.; *Science 320, 634 (2008);*

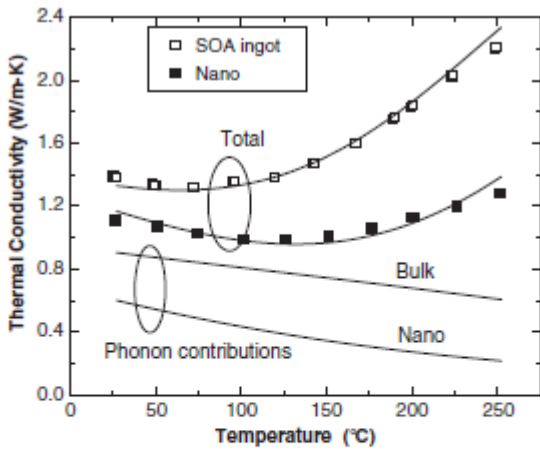
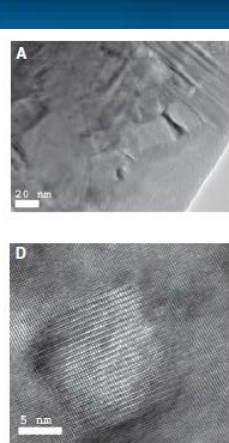
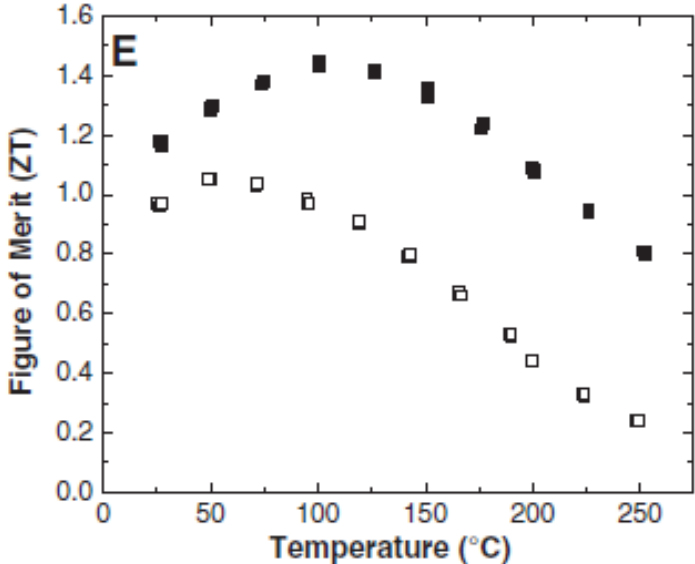


Fig. 4. Thermal conductivity of $\text{Bi}_x\text{Sb}_{2-x}\text{Te}_3$ NC bulk alloy. White and black squares represent the experimental results for an SOA ingot and our NC bulk alloys, respectively. Solid lines represent the corresponding calculations of the total (top curves) and lattice (bottom curves) contribution to the thermal conductivity, respectively.

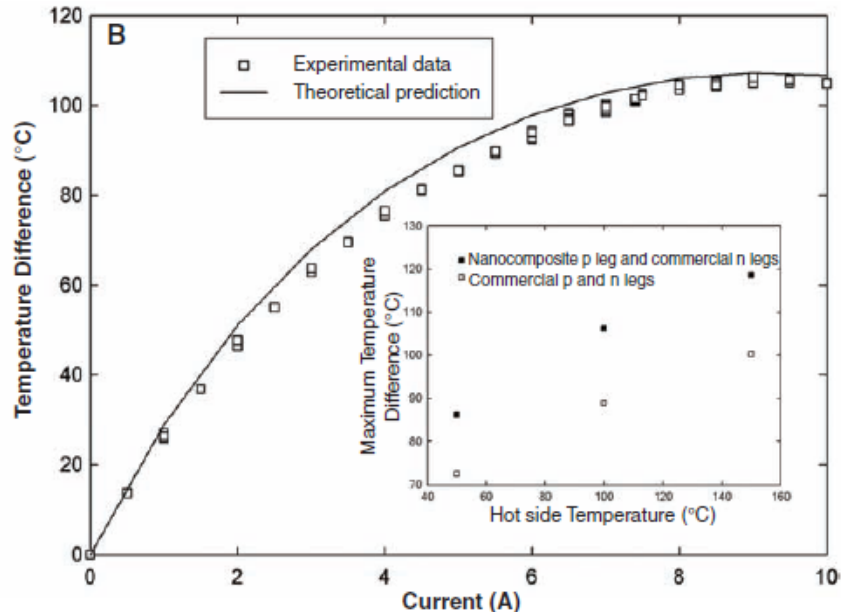


Fig. 5. (A) Experimental setup of the device cooling test. Two thermoelectric legs were mounted onto 6.5-mm-thick copper blocks and then bridged by a top copper plate. Two cold-side thermocouples were soldered into small holes drilled on both ends of the top copper plate. Hot-side thermocouples were soldered on the edge of each copper block. (B) Cooling test results with the hot side fixed at 100°C. The inset compares the maximum temperature difference of two unicouples with hot-side temperatures set at 50°, 100°, and 150°C.

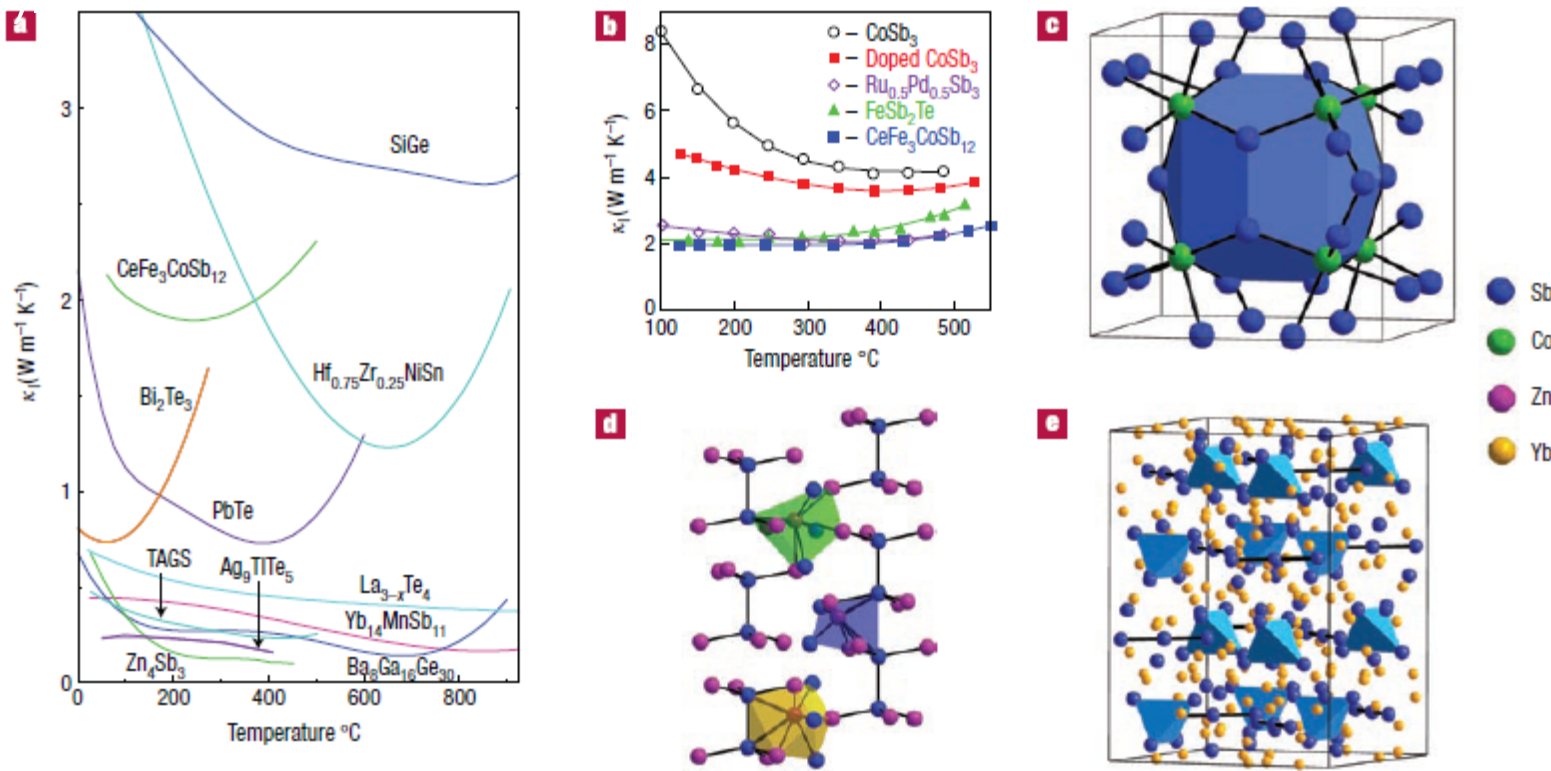


Figure 2 Complex crystal structures that yield low lattice thermal conductivity. **a**, Extremely low thermal conductivities are found in the recently identified complex material systems (such as Yb₁₄MnSb₁₁, ref. 45; CeFe₃CoSb₁₂, ref. 34; Ba_{0.9}Ga_{1.0}Ge_{3.0}, ref. 79; and Zn₄Sb₃, ref. 80; Ag₉TlTe₅, ref. 40; and La_{3-x}Te₄, Caltech unpublished data) compared with most state-of-the-art thermoelectric alloys (Bi₂Te₃, Caltech unpublished data; PbTe, ref. 81; TAGS, ref. 69; SiGe, ref. 82 or the half-Heusler alloy Hf_{0.75}Zr_{0.25}NiSn, ref. 83). **b**, The high thermal conductivity of CoSb₃ is lowered when the electrical conductivity is optimized by doping (doped CoSb₃). The thermal conductivity is further lowered by alloying on the Co (Ru_{0.5}Pd_{0.5}Sb₃) or Sb (FeSb₂Te) sites or by filling the void spaces (CeFe₃CoSb₁₂) (ref. 34). **c**, The skutterudite structure is composed of tilted octahedra of CoSb₃ creating large void spaces shown in blue. **d**, The room-temperature structure of Zn₄Sb₃ has a crystalline Sb sublattice (blue) and highly disordered Zn sublattice containing a variety of interstitial sites (in polyhedra) along with the primary sites (purple). **e**, The complexity of the Yb₁₄MnSb₁₁ unit cell is illustrated, with [Sb₃]⁷⁻ trimers, [MnSb₄]⁹⁻ tetrahedra, and isolated Sb anions. The Zintl formalism describes these units as covalently bound with electrons donated from the ionic Yb²⁺ sublattice (yellow).

Week 5: Recent Advances

- 5.1 • TE vs. TI: non-linear, lateral momentum conservation
- 5.2 • ErAs embedded nanoparticles in InGaAs
 - Reduce k_{lattice} by mid/long phonon scattering, doping the matrix, energy dependent scattering
- 5.3 • Optimum band structure
 - Classical TE materials: Bi_2Te_3 , PbTe, TAGS, SiGe
 - Chalcogenides: SPS Na(2%)-PbTe:SrTe(4%) ZT~2.2 at 900K
- 5.4 • Skutterudites, Clathrates, Half Heuslers, Oxides, Zintl phase, nano-composites
 - Spin Seebeck • Resonant state
- 5.5 • Carnot vs. Curzon-Ahlborn
 - Single level thermoelectrics
 - Some open questions (phase transition, coupled charge/energy transport, superlattice thermal conductivity, opto thermo electric devices)

Generic
thermoelectric device

